International Journal of Solids and Structures 51 (2014) 839–847

Contents lists available at ScienceDirect

International Journal of Solids and Structures

journal homepage: www.elsevier.com/locate/ijsolstr

Size effects due to secondary voids during ductile crack propagation

Geralf Hütter *, Lutz Zybell, Meinhard Kuna

TU Bergakademie Freiberg, Institute of Mechanics and Fluid Dynamics, Lampadiusstr. 4, 09596 Freiberg, Germany

ARTICLE INFO

Article history:
Received 9 September 2013
Received in revised form 6 November 2013
Available online 28 November 2013

Keywords:
Ductile fracture
Secondary voids
Discrete voids
Finite element analysis
Void growth and coalescence
Small-scale yielding

ABSTRACT

In the present study the size-effect due to a secondary void population during ductile fracture is investigated. Discrete primary voids are resolved in the process zone at the crack tip. A non-local GTN model is employed to describe the evolution of the secondary voids in the intervoid ligaments. The non-local GTN model contains an intrinsic length scale related to the size of the secondary voids. Hence, the ratio of the size of the primary and that of the secondary voids can be varied. The results show that small secondary voids can toughen the material. Such a behavior is in contrast to the prediction of cell model simulations. A theoretical reasoning of this effect and conclusions are given.

1. Introduction

Ductile failure is an important mechanism for the fracture of metals. The mechanism comprises the nucleation of microscopic voids at inclusions or second-phase particles, the growth of these voids and their coalescence. In many engineering metals different types of nuclei of void formation are present which differ typically in size, volume fraction and conditions of nucleation. They are mostly termed as populations of void nuclei. For instance, typical steels contain both, relatively weak inclusions such as manganese sulfide (MnS) inclusions and much smaller but harder carbide particles. The MnS inclusions are loosely bonded and nucleate voids early in the deformation process, whereas the debonding of the smaller carbides requires considerably higher plastic deformations. A corresponding fracture surface is shown in Fig. 1. Due to the relevance in engineering applications, the modeling of the ductile mechanism has attracted a lot of research efforts. In the following only a few key studies shall be discussed. Extensive reviews can be found in Tvergaard (1989), Benzerga and Leblond (2010) and Besson (2010).

The most widely used constitutive model to describe the void growth stage of the ductile mechanism was derived by Gurson (1977) by means of an analytical homogenization of a unit cell with ideal plastic matrix material. Here, the void volume fraction is introduced as intrinsic variable. Chu and Needleman (1980) presented an approach to incorporate the nucleation of voids. Tvergaard (1981, 1982) modified the model based on numerical simulations of a similar arrangement but with hardening matrix material (so-called cell model simulations). Furthermore, Tvergaard and Needleman (1984) extended the model to account for the stage of void coalescence. This model is today known as the Gurson–Tvergaard–Needleman model, abbreviated GTN.

In the nucleation approach by Chu and Needleman (1980), nucleated voids are added directly to the void volume fraction. Primary and secondary voids cannot be distinguished afterward. More sophisticated approaches were presented in Fabrègue and Pardoen (2008) and Perrin and Leblond (1990).

In many engineering metals one of the populations of voids nucleates early and at larger nuclei as described above. That is why this so called primary population is modeled in many studies (Tvergaard, 1982; Brocks et al., 1995; Fabrègue and Pardoen, 2008, among many others) as a priori existing and discrete void in a cell model whereas the secondary voids are incorporated in a smeared sense by employing the GTN model for the matrix material. The secondary voids affect mainly the initiation of the coalescence stage (Fabrègue and Pardoen, 2008).

In cell model simulations, the deformation state is assumed to be homogeneous with respect to the primary void. However, for practical applications the situation in front of a macroscopic crack tip is of great interest as well. Here, the deformations are highly non-homogeneous as sketched in Fig. 2. This problem was addressed by numerous researchers who resolved discretely a single void or several voids in front of the crack tip (see e.g. Aravas and McMeeking (1985), Gu (2000), Tvergaard and Hutchinson (2002), Gao et al. (2005), Petti and Dodds (2005), Tvergaard (2007), Chew et al. (2007), Hütter et al. (2012), Hütter et al. (2013) and Sreeramulu et al. (2013)). Aoki et al. (1984) and Aravas and McMeeking

* Corresponding author. Tel.: +49 3731393496.
E-mail address: Geralf.Huetter@imfd.tu-freiberg.de (G. Hütter).

0020-7683/$ - see front matter © 2013 Elsevier Ltd. All rights reserved.
http://dx.doi.org/10.1016/j.ijsolstr.2013.11.012

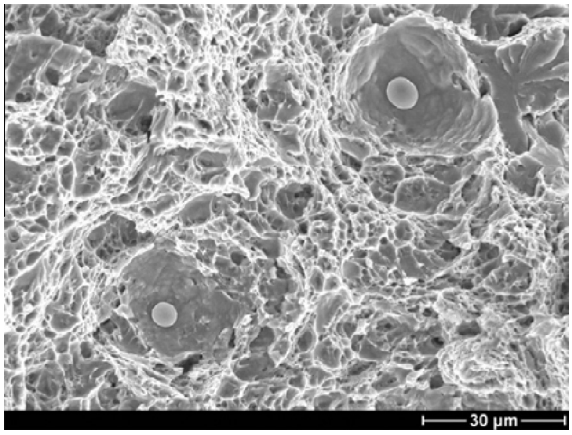

Fig. 1. Fracture surface after ductile failure in a pressure vessel steel (Seidenfuss et al., 2011).

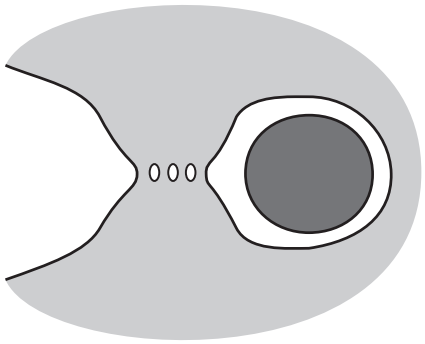

Fig. 2. Growth of secondary voids in front of a crack tip.

(1985) employed secondary voids in such a model by describing the matrix material by the GTN model as in the mentioned cell model simulations. In a similar approach the complete and compact domain is described by the GTN model but with islands of higher nucleable void volume fraction representing the primary voids (see e.g. Needleman and Tvergaard (1987) and Tvergaard and Needleman (2006)).

All of the aforementioned studies have in common that they incorporate the secondary voids only by their volume fraction within the theory of simple materials[1] and can thus not account for effects of the size of the secondary voids. This has the consequence that the respective boundary value problem has no physically meaningful solution if the growth of the secondary voids induces softening. This fact leads to the well-known problem of mesh-dependent results in corresponding finite element implementations.

This problem was addressed in Tvergaard and Needleman (1995) and Zybell et al. (in press) by using a non-local extension of the GTN-model for the secondary voids in the matrix material in cell model simulations. In non-local models an intrinsic length scale enters the constitutive description. This length is directly related to the spacing of the secondary voids. The results of the cell model simulations show that the smaller the secondary voids are compared to the primary ones, the earlier the primary voids coalesce.

Vernerey et al. (2008) presented a material model within the theory of micromorphic media that accounts for the size of the secondary voids, too. This model was used in Tian et al. (2010) together with discrete primary voids or islands of nucleable porosity at a crack tip to model crack propagation. These investigations focus on the simulation of the fracture initiation in a particular material, i.e. with stochastically aligned nuclei. The effect of the size of the secondary voids is not investigated. Size effects not due to secondary voids but due to gradient hardening of the matrix material were investigated in cell models (Niordson and Tvergaard, 2007) and with discrete voids at the crack tip (Tvergaard and Niordson, 2008). In both cases it is found that the void growth is retarded if the size of the voids is comparable to the characteristic length scale of the matrix material.

In the present study the size effect due to secondary voids during crack initiation and propagation is investigated in a two-dimensional model. For this purpose a number of discrete voids is resolved in front of a crack tip. The matrix material is described by the non-local GTN model by Linse et. al. (Linse et al., 2012; Hütter et al., 2013). This model belongs to the class of micromorphic media as well (Forest, 2009). A systematic parameter study is performed with respect to the size of the secondary voids and the nucleation parameters.

The paper is organized as follows. In Section 2 the employed model is presented. The global model of crack propagation is outlined in Section 2.1 before details of the non-local GTN model and of the numerical implementation are given in Sections 2.2 and 2.3. In Section 3 the model is preliminarily investigated in cell model computations before the actual fracture behavior is addressed in Section 4. The results are discussed in Section 5. Finally, Section 6 gives a summary and an outlook.

2. Model

2.1. Global model

The model to be investigated is sketched in Fig. 3. A number of regularly aligned and initially present primary voids of initial distance X_1 and volume fraction

$$f_{10} = \pi\left(\frac{R_1}{X_1}\right)^2 \tag{1}$$

are resolved discretely in the process zone. Here and in the following a subscript 1 refers to the primary void population and correspondingly 2 to the secondary one. Due to the computational effort, a plane model under plane strain conditions is considered thus corresponding to an infinitely thick specimen with cylindrical primary voids whose axes are aligned parallel to the crack front.

The matrix material between the voids is described by the non-local GTN model by Linse et al. (Hütter et al., 2013; Linse et al., 2012). Details of this model will be given in Section 2.2. This way the secondary voids are incorporated in a smeared way with the volume fraction f_2 and the intrinsic material length l_2. The smeared representation requires that the secondary voids are considerably smaller than the primary ones. The length l_2 is directly related to the distance of the secondary voids. Thus, the model is consistent only if l_2 is considerably smaller than X_1. However, no hard border between admissible and inadmissible values of the ratio l_2/X_1 can be given. For this reason most of the following simulations are performed in the regime $l_2/X_1 \leq 0.4$. Some results with a higher value of this ratio will be given which have merely a mathematical character as will be discussed at appropriate positions. The secondary voids can be initially present or can nucleate during the deformation process. Young's modulus and Poisson ratio of the matrix material are denoted as E and ν.

The material outside the process zone is described consistently by the GTN model (which is a special case of the non-local GTN

[1] The current state of a material point depends on the history of the deformation gradient at this point only.

model) thus incorporating the primary voids and their potential growth in a homogenized way by the void volume fraction f_1. This is an important issue as found in Hütter et al. (2012). The void growth around the process zone, although being small in magnitude, shields the process zone from hydrostatic stresses thus retarding the fracture initiation significantly. The GTN model cannot describe the inhomogeneous deformation states and loading histories directly around the process zone adequately. Thus, a number of layers of discrete voids has to be incorporated. For a consistent transition from the discretely resolved region to the homogenized one, some layers of discrete voids have to be incorporated (Hütter et al., 2012). The particular number will be given in Section 2.3.

As the material behavior in the outer region shall reflect that of the porous medium in a homogenized way, the effective Young's modulus E_{eff} of the outer region has to be smaller than the one of the matrix material. The effective elastic properties E_{eff} and ν_{eff} of a material with cylindrical voids under plane strain can be found in text books (e.g. Gross and Seelig, 2006). The particular values depend on the primary void volume fraction f_{10} and are summarized in Table 1. The change of the elastic properties with ongoing void growth is not taken into account. If not stated otherwise an initial primary void volume fraction $f_{10} = 0.014$ ($R_1/X_1 = 1/15$) is used for the following simulations. This value was used in many preceding studies in the literature (Tvergaard and Hutchinson, 2002; Tvergaard, 2007; Hütter et al., 2012, 2013; Tvergaard and Niordson, 2008).

In the following, the limiting case of a semi-infinite crack is considered in order to exclude possible effects of the geometry of a particular specimen. In this case of ideal small-scale yielding, the elastic far-field is uniquely defined by the stress-intensity factor K_I. Thus, the energy-release rate of the far-field is obtained as

$$J = \frac{K_I^2\left(1-\nu_{\text{eff}}^2\right)}{E_{\text{eff}}}. \tag{2}$$

Under certain conditions ligaments may rupture abruptly within a dynamic process as will be seen and explained in Section 4. Thus, the mass density ρ has to be incorporated. However, in order to exclude possible effects of the loading rate, the load K_I shall be applied quasi-statically. This means, that the time scale of loading τ_{L} is large compared to that time which elastic waves need to pass characteristic distances of the problem. In the considered case of the semi-infinite crack, this concerns only the material length scales X_1 and l_2. The former is typically the larger one and it has to be ensured that

$$\tau_{\text{L}} \gg X_1/c_{\text{s}} \tag{3}$$

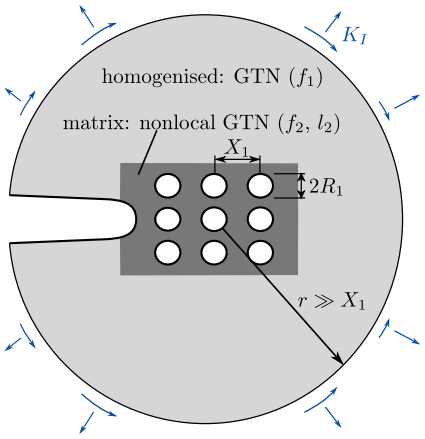

Fig. 3. Semi-infinite crack with resolved process zone.

Table 1
Effective elastic properties for a Poisson ratio of the matrix $\nu = 0.3$.

f_{10}	0.014	0.056
E_{eff}/E	0.96	0.86
ν_{eff}	0.293	0.290

holds. Therein, $c_{\text{s}} = \sqrt{E/[2(1+\nu)\rho]}$ is the speed of the slower shear waves. In the numerical implementation of the described model stronger restrictions than (3) hold as will be explained in Section 2.3.

The presented model incorporates the limit case that no secondary voids are present. Then, the matrix material behaves as Mises-plastic. This case was investigated in the preceding study (Hütter et al., 2012). Although no material separation occurs, it was found that at appropriate loading the geometric softening of the intervoid ligaments after their plastic collapse is sufficient to propagate the crack effectively. For this reason the amount of crack extension Δa was measured as the distance from the initial crack tip to the center of the currently active zone of geometric softening.

In the present study the width W_i of each intervoid ligament i decreases during deformation starting from $W_0 = X_1 - 2R_1$. Due to the growth of secondary voids now the intervoid ligaments can have a width W_i^{rem} behind the active softening. In the mentioned case of absent secondary voids W_i^{rem} is zero. In order to be compatible with the aforementioned study and to be able to treat the limiting case $W_i^{\text{rem}} = 0$, the crack extension is defined as

$$\Delta a = X_1 \sum_{i=1}^{n_{\text{lig}}} \frac{1 - W_i/W_0}{1 - W_i^{\text{rem}}/W_0}. \tag{4}$$

The definition is constructed such that a ligament that has still its initial width $W_i = W_0$ does not contribute to Δa whereas a fully failed ligament $W_i = W_i^{\text{rem}}$ is counted as a crack extension of a void distance X_1. The definition is illustrated in Fig. 4.

2.2. Non-local GTN model

The non-local extension of the GTN model by Linse et. al. (Hütter et al., 2013; Linse et al., 2012) is used for the matrix material. Here, only a brief overview of this model is given. For details the reader is referred to the mentioned publications. In the non-local extension, the yield condition

$$\left(\frac{\sigma_{\text{eq}}}{\bar{\sigma}}\right)^2 + 2q_1 f \cosh\left(\frac{3q_2}{2}\frac{\sigma_{\text{m}}}{\bar{\sigma}}\right) - 1 - (q_1 f)^2 \leq 0 \tag{5}$$

of the original GTN model is retained as well as the balances of momentum and of moment of momentum. The quantities $\sigma_{\text{eq}}, \sigma_{\text{m}}$ and $\bar{\sigma}$ denote the Mises, the hydrostatic and the effective yield stress of the matrix material, respectively. The standard values $q_1 = 1.5$ and $q_2 = 1.0$ of the fitting parameters are used in the following. The effective void volume fraction f coincides with the actual one f during stable void growth but takes a larger value in the void coalescence stage which initiates when f reaches the value f_{c}:

$$f^* = \begin{cases} f & f \leqslant f_{\text{c}} \\ f_{\text{c}} + (f - f_{\text{c}})K & f_{\text{c}} < f \leqslant f_{\text{f}} \\ f_{\text{u}} & f_{\text{f}} < f \end{cases} \tag{6}$$

$$\text{with } K = \frac{f_{\text{u}} - f_{\text{c}}}{f_{\text{f}} - f_{\text{c}}}, \quad f_{\text{u}} = \frac{1}{q_1}.$$

The term f_{f} is the void volume fraction at which the material looses its stress-carrying capacity completely. The GTN-model merges into the case of Mises plasticity for $f = 0$. Void growth and void nucleation contribute to the evolution of the void volume fraction:

$$\dot{f} = \dot{f}_G + \dot{f}_N \tag{7}$$

The classical Chu–Needleman approach (Chu and Needleman, 1980)

$$\dot{f}_N = \frac{f_n}{s_N\sqrt{2\pi}} \exp\left[-\frac{1}{2}\left(\frac{\bar{\varepsilon}-\varepsilon_N}{s_N}\right)^2\right]\dot{\bar{\varepsilon}} \tag{8}$$

with nucleation driven by the equivalent plastic strain $\bar{\varepsilon}$ is used for the nucleation since the latter applies to the matrix material where the secondary voids are the only void population. Therein, f_n is the nucleable porosity. The terms ε_N and s_N refer to the mean equivalent plastic strain at which nucleation takes place and the standard deviation thereof. The evolution equation for $\bar{\varepsilon}$ is well-known and not repeated here. The non-local modification concerns the equation for void growth:

$$\dot{f}_G = (1-f)\dot{\varepsilon}_{nl}. \tag{9}$$

Here, the volumetric plastic strain ε_{pl}^{vol} is replaced by its non-local counterpart ε_{nl}. The latter is introduced in an implicitly gradient-enriched formulation by the partial differential equation of Helmholtz type

$$\varepsilon_{nl} - \nabla\cdot\left(l_{nl}^2\nabla\varepsilon_{nl}\right) = \varepsilon_{pl}^{vol}. \tag{10}$$

The Nabla operator ∇ refers to the current configuration. The length l_{nl} being related to the void distance enters as prefactor of the gradient terms. For the secondary voids in the matrix between the discrete primary voids, this length is termed as l_2. In the outer region, where the material behavior is treated completely homogenized, the gradients are weak compared to the distance of the primary voids so that the gradient terms can be neglected in this region. This leads to the classical GTN model by setting l_{nl} to zero there (compare Fig. 3). The situation is different in the process zone when l_2 is small compared to the distance X_1 of primary voids. Here, also small values of l_2 are significant since l_2 limits the size of the zone of localization of void growth and coalescence. Regarding real materials it has to be mentioned that small value of the ratio l_2/X_1 mean that the length l_2 lies in the range of a few micrometers or even below. Such length scales are already comparable to the mean-free-path of dislocations so that strain gradient effects appear. Eq. (10) does not incorporate such effects. This fact has to be kept in mind and is discussed in Section 5.

Boundary conditions have to be specified for the partial differential equation (10). The trivial natural boundary condition is prescribed at free surfaces ensuring that the overall mean values of local and non-local volumetric plastic strains are equal if no material fails completely. If material fails completely, an essential boundary condition is specified at the respective regions. This means that the non-local strain is fixed at the moment of failure (Hütter et al., 2013). Then, no nucleation occurs anymore and thus also the void volume fraction is fixed at the final value f_f which is physically reasonable (and is assumed also in the classical GTN model).

The last "ingredient" of the model is the dependence of the matrix yield stress $\bar{\sigma}$ on the equivalent plastic $\bar{\varepsilon}$ strain, i.e. the hardening law. Here, a well-established one-parametric power law is utilized given implicitly by

$$\frac{\bar{\sigma}}{\sigma_0} = \left(\frac{\bar{\sigma}}{\sigma_0} + \frac{E}{\sigma_0}\bar{\varepsilon}\right)^N. \tag{11}$$

The symbols σ_0 and N denote the initial yield stress and the hardening exponent, respectively. In the following the elastic-plastic material parameters are set to $\sigma_0 = 0.003E, N = 0.1$ and $\nu = 0.3$. These parameters correspond to the behavior of typical medium strength engineering metals and are used in many studies in the literature which deal with the processes at the crack tip, e.g. in Tvergaard and Hutchinson (2002), Tvergaard (2007) and McMeeking (1977). For the material behavior in the outer region of the fracture model, a slight calibration of the hardening law $\bar{\sigma}(\bar{\varepsilon})$ provided for the outer region is necessary to match the homogenized behavior of the discrete void region, see Hütter et al. (2012).

In the following simulations a potential volume fraction of secondary voids of 0.01 is assumed. The secondary voids are assumed to be initially present ($f_{20} = 0.01, f_{n2} = 0$) or to nucleate ($f_{20} = 0, f_{n2} = 0.01$) after different levels of straining ($\varepsilon_{N2} = 0.3$ or $\varepsilon_{N2} = 0.6$ with $s_{N2} = 0.1$). The corresponding simulations are denominated in the following as $\varepsilon_{N2} = 0$ (initially present), $\varepsilon_{N2} = 0.3$ and $\varepsilon_{N2} = 0.6$, respectively. For comparison simulations without any secondary voids ($f_{20} = 0, f_{n2} = 0$) will be performed which will be referred to as $f_2 = 0$. The employed values for void nucleation lie in the mean of the values from literature (Brocks et al., 1995; Aravas and McMeeking, 1985; Needleman and Tvergaard, 1987; Gao and Kim, 2006) which range from $f_{n2} = 0.004\ldots0.04$ and $\varepsilon_{N2} = 0.1\ldots0.8$ at $s_{N2} = 0.1$. If not stated otherwise, a coalescence porosity $f_{c2} = 0.05$ with $f_{f2} = 0.13$ is used from Koplik and Needleman (1988)) together with an intermediate nucleation strain of $\varepsilon_{N2} = 0.3$.

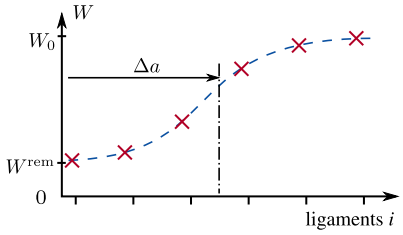

Fig. 4. Measure of crack extension.

2.3. Numerical implementation

In a finite element implementation of the fracture model described in Section 2.1, a finite region has to be spatially discretized. This is often termed a boundary layer model. For symmetry reasons only half of the model needs to be considered in the FE-model. A boundary layer of radius $A_0 = 4500X_1$ is spatially discretized. Ten layers of 40 voids each are resolved discretely in the half model as derived in Hütter et al. (2012). Elements with quadratic ansatz functions for geometry and displacements and linear ones for the non-local strain ε_{nl} are employed with a reduced integration scheme. The essential boundary condition at failure is implemented by means of a penalty formulation, see Hütter et al. (2013).

The choice of the element size h in the intervoid ligaments requires several considerations. Firstly, the elements have to be smaller than the intrinsic length scale l_2. The convergence study in Linse et al. (2012) showed that $h \lesssim 0.25\,l_2$ has to hold. Furthermore, simulations with late nucleation of secondary voids shall be performed. In this case large plastic deformations occur before the secondary voids nucleate. The mentioned restriction of h applies to the current configuration wherein the PDE (10) is formulated. Thus, the mesh is constructed in a way that the highly strained elements in the center of the intervoid ligaments are initially flat while they approach an aspect ratio near unity when the secondary voids nucleate. A typical mesh near the crack tip used for the simulations is shown in Fig. 5. The largest width of the element in the center of the intervoid ligament is $h = 0.04X_1$.

In order to ensure quasi-static loading conditions, requirement (3) does not apply to the material length scale X_1 only. Merely, it is necessary that the time the elastic waves need to pass the radius A_0 of the boundary layer is small compared to the time scale of loading τ_L, too. For this purpose the mass density ρ is specified such

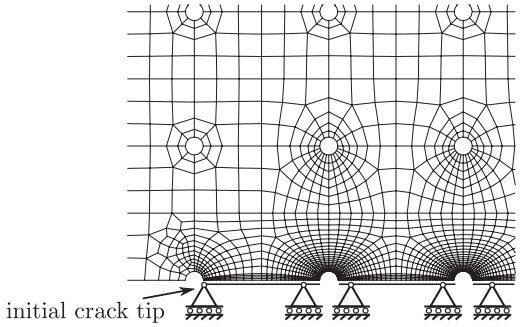

Fig. 5. Finite element mesh near the crack tip.

that $A_0/c_s = 0.001\tau_L$ holds. The described boundary value problem is solved numerically with the commercial FE-code Abaqus/Standard. A dynamic simulation with implicit time integration is performed.

3. Size effect in cell model simulations

Before the presented fracture model is investigated, a preliminary investigation is devoted to some cell model simulations. The results shall be used to compare the size effects in cell models, i.e. under homogeneous straining, and under the highly inhomogeneous conditions during fracture. The used cell model is shown in Fig. 6. Consistent with the envisaged fracture simulations, a two-dimensional model under plane-strain conditions is employed. The load, i.e. the mesoscopic stresses Σ_{xx} and Σ_{yy}, are applied as usual by an arc-length method. In this plane model, only the biaxiality ratio Σ_{xx}/Σ_{yy} can be varied. Stress–strain curves for the parameter set with $f_{20} = 0, f_{n2} = 0.01$ and $\varepsilon_{N2} = 0.3$ are shown in Fig. 7 for different values of the characteristic length scale of the secondary voids l_2/X_1 at different levels of biaxiality in terms of the major principal stress and strain as in Tvergaard (1981). For a given (nucleable or initially present) volume fraction of secondary voids, the distance and thus the size of secondary voids is proportional to l_2. Thus, the value l_2 will be associated in the following with the size of the secondary voids. Fig. 7 contains (as most of the following figures) for comparison the respective results for an ideal ductile matrix, i.e. in absence of secondary voids $f_2 = 0$. The stress–strain curves for uniaxial loading (Fig. 7(a)) show that the secondary voids affect only the very late stage of void coalescence. With increasing biaxiality Σ_{xx}/Σ_{yy} the effect of the secondary voids increases. However, still only the stage of void coalescence is affected with a clear tendency: the smaller the secondary voids are, the earlier the voids coalesce. These tendencies apply also for other nucleation parameters (not shown here) and are consistent with the literature mentioned in the introduction.

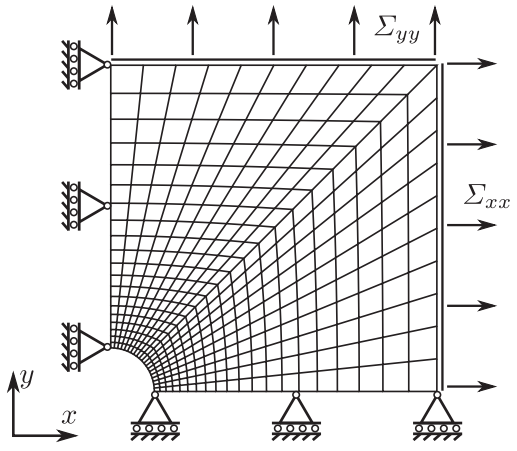

Fig. 6. Cell model.

4. Results for fracture

Now, the described fracture model is employed to investigate the influence of the size of the secondary voids on ductile fracture. For this purpose the ratio l_2/X_1 is varied. Again, the parameter set with $f_{20} = 0, f_{n2} = 0.01$ and $\varepsilon_{N2} = 0.3$ is investigated first. The distribution of the void volume fraction of secondary voids f_2 in the intervoid ligaments after some amount of crack extension is shown in Fig. 8. The FE-results of the half model are mirrored for illustration purpose. As expected, the zone of void growth is wider for the larger secondary voids $l_2/X_1 = 0.40$. Furthermore, in this case the intervoid ligaments experience higher straining before rupture compared to $l_2/X_1 = 0.20$ in Fig. 8(a). Consequently, the primary voids in the wake behind the current crack tip are larger (corresponding to a smaller remaining width of the intervoid ligaments W^{rem}). This finding is consistent with the cell model simulations as presented before in Section 3. In addition, Fig. 8 shows that for small secondary voids $l_2/X_1 = 0.20$ the crack propagates by a void-by-void mechanism since the intervoid ligaments rupture abruptly. In contrast, for larger secondary voids $l_2/X_1 = 0.40$ in Fig. 8(b), the active process zone encompasses several voids (multiple-void mechanism).

The corresponding crack growth resistance curves (R-curves) for several ratios l_2/X_1 are plotted in Fig. 9. Again, the figure incorporates the curve for an ideal ductile matrix $f_2 = 0$ (i.e. $f_{20} = f_n = 0$) from (Hütter et al., 2012). As expected from the cell model simulations, the diagram shows that the smaller the secondary voids are compared to the primary voids (i.e. the lower l_2/X_1 is), the earlier fracture initiates. Furthermore, for small secondary voids $l_2/X_1 = 0.20$ and $l_2/X_1 = 0.25$ the R-curves exhibit steps due to the void-by-void mechanism. For increasing values of l_2/X_1 the computed R-curves become smoother and converge towards the ideal ductile one as expected as well. The reason is that the local strains in the intervoid ligaments are "averaged out" (although the model is physically questionable then since the secondary voids cannot be incorporated smearedly with the non-local GTN model if they are as large as the primary ones or even larger).

Regarding the tearing behavior, it is highly remarkable that low values of l_2/X_1 lead to a high slope of the R-curve. This strong tearing makes the R-curves for low l_2/X_1 exceed the ideal ductile one by far after some crack extension Δa. Note that the transition from the void-by-void mechanism to the multiple-void mechanism takes place within a relatively narrow range between $l_2/X_1 = 0.25$ and $l_2/X_1 = 0.35$. The simulation with the value $l_2/X_1 = 0.30$ in between seems to balance on a knife's edge. Both mechanisms alternate leading to oscillations in the respective R-curve.

When going from $l_2/X_1 = 0.25$ to $l_2/X_1 = 0.20$ there is only a moderate change in the R-curves. It is expected that the computed R-curves converge towards a single one if the secondary voids become smaller and smaller, i.e. for $l_2/X_1 \to 0$. The reason is as follows: In this limit case the voids nucleate when the respective strain level is reached in the intervoid ligaments. But due to their small size this process corresponds directly to the formation of a crack in the center of the intervoid ligament. The fracture toughness of the intervoid ligament is determined by the size of the secondary voids. As this size decreases, the fracture toughness diminishes. Thus, for $l_2/X_1 \to 0$ the nucleation of (a sufficient amount of) secondary voids corresponds to the abrupt rupture of the intervoid ligament and the macroscopic fracture behavior is

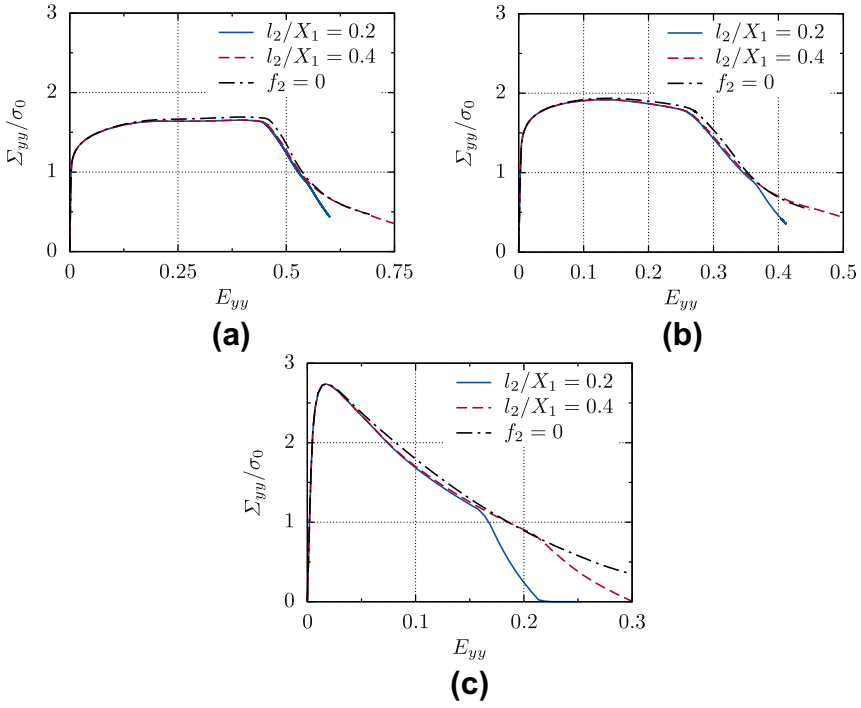

Fig. 7. Macroscopic stress–strain curves from cell model simulations under (a) uniaxial loading $\Sigma_{xx} = 0$, (b) low biaxiality $\Sigma_{xx}/\Sigma_{yy} = 0.25$ and (c) high biaxiality $\Sigma_{xx}/\Sigma_{yy} = 0.75$ ($\varepsilon_{N2} = 0.3$).

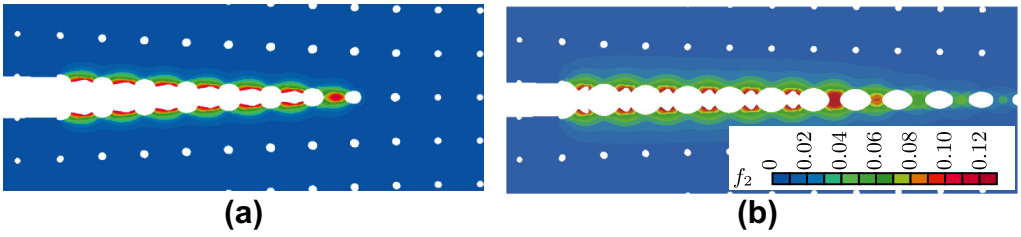

Fig. 8. Distribution of secondary void volume fraction f_2 in process zone after complete failure of the first six intervoid ligaments: Change from (a) void-by-void mechanism for $l_2/X_1 = 0.20$ to (b) multiple void interaction for $l_2/X_1 = 0.40$.

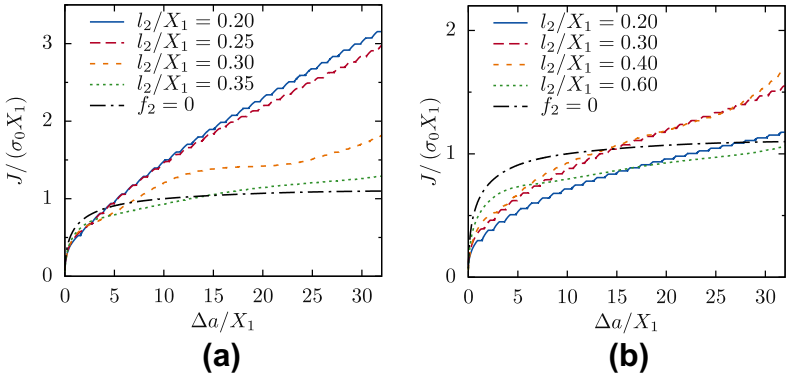

Fig. 9. Influence of the relative size of secondary voids l_2/X_1 on crack growth resistance curves for (a) nucleating ($\varepsilon_N = 0.3$) and (b) initially present secondary voids ($\varepsilon_N = 0$). The result for an ideal ductile matrix $f_2 = 0$ from Hütter et al. (2012) is included for comparison.

determined by the pre-nucleation plastic behavior of the matrix material in the intervoid ligaments only. However, this limit case can hardly be assessed by the present model since the maximum allowed element size is proportional to l_2, see Section 2.3. This means that more and more elements are necessary with decreasing l_2/X_1.

Fig. 9(b) shows again the predicted R-curves for varying l_2/X_1 now for initially present secondary voids ($\varepsilon_N = 0$). The effect of l_2/X_1 on the initial tearing is similar to the previous case, i.e. a lower ratio l_2/X_1 leads to a stronger tearing. Furthermore, the ideal ductile curve $f_2 = 0$ is reached for large secondary voids as well. However, Fig. 9(b) shows also that initially present small

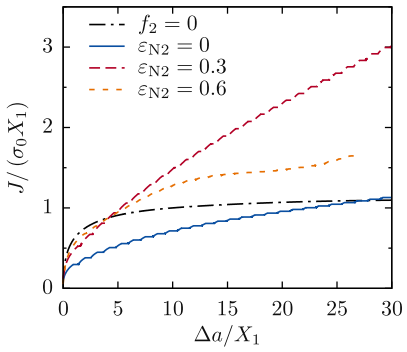

Fig. 10. Influence of ε_{N2} on crack growth resistance curve ($f_{10} = 0.014, l_2/X_1 = 0.20$).

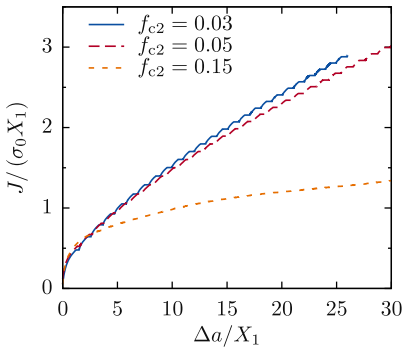

Fig. 12. Influence of f_c on crack growth resistance curve ($f_{10} = 0.014, \varepsilon_{N2} = 0.3, l_2/X_1 = 0.20$).

secondary voids reduce the fracture initiation toughness considerably. The effects of higher initial tearing and lower fracture initiation toughness result in *R*-curves which intersect the one of the ideal ductile matrix $f_2 = 0$ after a larger amount of crack extension Δa compared to the case of nucleating secondary voids in Fig. 9(a).

In Fig. 10 the *R*-curves obtained with different values of the nucleation strain ε_{N2} are compared directly for a fixed size ratio. Namely, the value $l_2/X_1 = 0.2$ is used since a large effect of secondary voids was found with it above. Again, the curves for the ideal ductile matrix material ($f_2 = 0$) is incorporated. The results confirm the finding that the later the voids nucleate, the larger is the fracture initiation toughness. However, the trend with respect to the tearing is not unique. The highest slope of the *R*-curve after fracture initiation is obtained for the employed ratio $l_2/X_1 = 0.2$ with $\varepsilon_{N2} = 0.3$, i.e. when the voids nucleate in the intermediate stage of straining of the intervoid ligaments.

The obtained values of the fracture initiation toughness J_c are plotted in Fig. 11 against the relative size of the secondary voids. The fracture initiation toughness J_c is defined as the value J at the kink in the CTOD-J curve according to (Gu, 2000). As discussed, two limit cases can be identified. These are the ideal ductile one for $l_2/X_1 \to \infty$, which is independent of the nucleation parameters, and the one of immediate rupture of the intervoid ligaments for $l_2/X_1 \to 0$. The latter is physically critical and difficult to be assessed numerically as already explained. Nevertheless, it becomes already apparent in Fig. 11. The immediate rupture for $l_2/X_1 \to 0$ occurs the earlier, the earlier the voids nucleate. Thus, the difference with respect to J_c between both limit cases is affected correspondingly and the effect of l_2/X_1 on J_c is the stronger the earlier the voids nucleate.

Next, the influence of other parameters of the model is investigated. Firstly, f_{c2} is addressed. This parameter describes

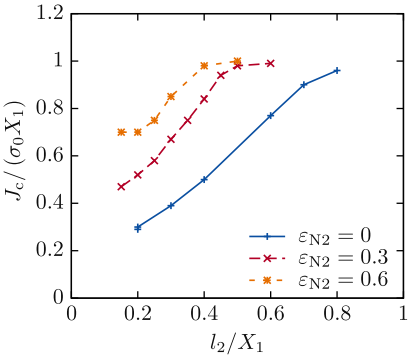

Fig. 11. Influence of l_2/X_1 on fracture initiation toughness for different nucleation parameters.

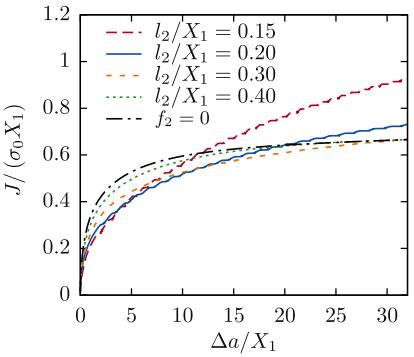

Fig. 13. Influence of the relative size of secondary voids l_2/X_1 on crack growth resistance curves for larger primary void volume fraction $f_{10} = 0.056$ ($\varepsilon_{N2} = 0.3$).

the coalescence behavior of the secondary voids. A relative size of the secondary voids $l_2 = 0.20X_1$ is used again. For this value it was found above that the secondary voids have a strong influence. The values of f_{f2} corresponding to the respective values of f_{c2} are taken from Hütter et al. (2013). The computed *R*-curves are plotted in Fig. 12. The results show that the lower f_{c2} is, the earlier fracture initiates, a behavior that is plausible. The effect on the predicted tearing behavior is opposite. This is remarkable since it was found in Hütter et al. (2013) that for the homogeneous non-local GTN-material alone a higher f_{c2} leads to a stronger tearing. Apparently, the transition to the void-by-void mechanism due to earlier rupture of the intervoid ligaments overcompensates this effect.

Finally, in Fig. 13 the *R*-curves for a larger primary void volume fraction of $f_{10} = 0.056$ are shown. The same nucleation parameters are used as before but the relative size l_2/X_1 of the secondary voids is varied. It is found that with this larger primary void volume fraction, changes in l_2/X_1 have a considerably weaker effect compared to $f_{10} = 0.014$ in Fig. 9(a). The reason for this weaker dependence is presumably that with this higher f_{10} the active softening zone encompasses more voids in the ideal ductile case as shown in Tvergaard and Hutchinson (2002). Thus, the multiple-void mechanism is less susceptible to perturbations.

5. Discussion

The results show that the present model predicts a strong toughening effect by secondary voids that are more densely distributed at the same void volume fraction f_2. One reason is the transition from the multiple-void mechanism to the single void mechanism. In a companion study (Hütter, 2013) a similar finding is reported if cleavage acts as secondary damage mechanism. Tvergaard and Hutchinson (Tvergaard and Hutchinson, 2002;

Tvergaard, 2007) used a fracture model with several discrete voids in front of the crack tip, too, with Mises plastic matrix material. They investigated the effect of the void volume fraction and observed a toughening with decreasing void volume fraction and discovered the interrelationship between the toughening and the transition from the multiple-void mechanism to the single-void mechanism. These authors assumed an intervoid ligament to be completely damaged when it reached a critical value of the relative necking (which is equivalent to a critical mean longitudinal strain of the ligament for volume preserving plasticity). A node release technique was used in the FEM simulations to rupture the respective intervoid ligaments immediately. Such an approach corresponds to the limit case $l_2/X_1 \to 0$ of the present model discussed in the preceding section. It was argued in this preceding section that this limit case corresponds to an abrupt rupture of the respective intervoid ligament if the nucleation strain is reached. This is similar to the critical mean strain in the approach of Tvergaard and Hutchinson. Consequently, their model predicts a stronger tearing compared to the ideal ductile one in Hütter et al. (2012).

The reason for the toughening by the transition from the multiple-void mechanism to the single void mechanism can be found in the asymptotic analysis of the near-tip field of a growing crack in an elastic-plastic material by Rice et al. (1980). According to their analysis the opening δ_y of the crack face in a distance r from the current crack tip amounts to

$$\delta_y = r\beta\frac{\sigma_0}{E}\left[\frac{\alpha}{\beta}T_R + 1 + \ln\frac{R}{r}\right]. \tag{12}$$

Therein, α and β are dimensionless parameters to be determined from numerical analyzes. They amount to about $\alpha \approx 0.5$ and $\beta \approx 5$. The value R scales with the size of the plastic zone as $R = \lambda EJ/\sigma_0^2$ with $\lambda \approx 0.2$. The Paris tearing modulus is denoted as

$$T_R = \frac{E}{\sigma_0^2}\cdot\frac{\partial J}{\partial \Delta a} = \frac{E}{\sigma_0}\cdot\frac{\partial(J/(\sigma_0 X_1))}{\partial(\Delta a/X_1)}. \tag{13}$$

Solution (12) has an $r\ln r$ singularity which is weaker than the one of a stationary crack. Analyzing (12), Rice, Drugan and Sham concluded that if $T_R \gg 1$, there is a wide region in the plastic zone where T_R dominates the bracketed term in (12). Thus, δ_y is proportional to r in this region, i.e. the crack flanks remain planar. This is clearly the case in Fig. 8. In this case the slope of the flanks is proportional to the tearing modulus T_R. The planar flanks justify the introduction of the crack tip opening angle CTOA as measure of tearing whose tangent (which is practically equal to CTOA in the relevant range) is thus proportional to T_R.

Regarding now the present model under this point of view, the single-void mechanism leads to a steeper local profile of deformations, thus to a higher CTOA and thus to a higher tearing modulus. A second important issue is the relation between the initial tearing modulus and the saturation behavior of the R-curve. Eq. (12) can be rearranged to

$$\delta_y = r\beta\frac{\sigma_0}{E}\ln\frac{\bar{R}}{r} \tag{14}$$

with $\bar{R} = R\exp(1 + \alpha/\beta T_R)$. This representation exhibits a self-similar field whose "intensity" is given by $\bar{R}$. Rice, Drugan and Sham propose $\bar{R} = \text{const}$ as criterion for ongoing crack growth, i.e. that the near-tip field remains the same during crack propagation. The results of the present study are in agreement with this assumption. If now $\bar{R} = \text{const}$ is evaluated at fracture initiation at J_c with initial tearing modulus T_{R0} and at the steady-state $J = J_{ss}$ with $T_R = 0$ one finds that

$$\frac{J_{ss}}{J_c} = \exp\left(\frac{\alpha T_{R0}}{\beta}\right). \tag{15}$$

This means that the ratio J_{ss}/J_c between steady-state toughness and fracture initiation toughness scales exponentially with T_{R0}. This explains why the R-curves with lower fracture initiation toughness J_c but higher initial tearing T_{R0} outrun the ones of ideal ductile behavior. The T_{R0} is directly related to the gradients of the local fields over $\bar{R}$ (and thus proportional to CTOA under the discussed conditions). The exponential influence in (15), which arises in turn from the logarithmic singularity of the near-tip field of the moving crack, is the reason for the very strong effect of the transition from the multiple-void mechanism to the single-void mechanism.

At this point the question arises whether the present model reproduces the effect of secondary voids on this transition realistically. Gao et al., 2005 performed simulations with spherical voids embedded in Mises plastic material at the crack tip. Comparing their results with the mentioned study by Tvergaard and Hutchinson (2002) they found that the plane model, as used also in the present study, overestimates the single-void mechanism.

A second issue concerns the case of small secondary voids which was discussed mathematically as $l_2/X_1 \to 0$ above. For real materials this would correspond to submicron-sized voids. It is well-known from many studies that the plastic deformations in this regime are already influenced by strain-gradient effects, in particular the void nucleation and growth is delayed (see e.g. Niordson and Tvergaard (2007)). For this reason and due to the employed plane voids, it is to be expected that the present model overestimates the effect of the secondary voids.

6. Summary

In the present study the size-effect due to a secondary void population during ductile crack propagation is investigated. For this purpose the matrix material around the discrete primary voids is described by a non-local GTN model. The latter incorporates an intrinsic length being related to the mean distance (and thus to the size) of the secondary voids.

Cell model simulations with this approach yield the same tendency as known from literature: The smaller the secondary voids are compared to the primary one, the earlier the primary voids coalesce. In a corresponding fracture model with the same approach, i.e. a number of primary voids resolved discretely in the process zone with the non-local GTN model applied to the matrix material, the tendency is the same: The smaller the secondary voids are compared to the primary ones, the earlier fracture initiates. However, the tendency regarding tearing is opposite: Smaller secondary voids increase the tearing modulus and the crack growth resistance curves may outrun the corresponding one for ideal ductile matrix material. The reason is the transition from the mutiple-void mechanism for the ideal ductile matrix to the single-void mechanism if small secondary voids are present. Thus, the present model predicts that small secondary voids can effectively toughen a material. A theoretical reasoning for the strong size- effect with the secondary voids based on the near-field analysis by Rice et al. (1980) is given. However, regarding the quantitative predictions it is important to mention that the present model is planar corresponding to cylindrical primary voids and that no strain gradient effects are incorporated.

The conclusion has to be drawn that more attention has to be paid to secondary damage mechanisms during fracture. Cell models seem to be suitable to only a limited extent to address the corresponding effects. But probably planar models with discrete voids at the crack tip are insufficient, too, to describe the crack propagation beyond the fracture initiation as they are too sensitive with respect to secondary damage mechanisms of the ligaments between the primary voids. Further simulations with spherical primary voids in front of the crack tip are necessary to

address this question. Of course, such simulations are computationally much more expensive.

Acknowledgments

The financial support of this investigation by the Deutsche Forschungsgemeinschaft (German Science Foundation) under contracts KU 929/13-2 (Zybell), KU 929/14-2 (Hütter) and INST 267/81-1 FUGG (computing facilities) is gratefully acknowledged.

References

Aoki, S., Kishimoto, K., Takeya, A., Sakata, M., 1984. Effects of microvoids on crack blunting and initiation in ductile materials. Int. J. Fract. 24 (4), 267–278.
Aravas, N., McMeeking, R.M., 1985. Microvoid growth and failure in the ligament between a hole and a blunt crack tip. Int. J. Fract. 29 (1), 21–38.
Benzerga, A.A., Leblond, J.-B., 2010. Ductile fracture by void growth to coalescence. Adv. Appl. Mech. 44, 169–305.
Besson, J., 2010. Continuum models of ductile fracture: a review. Int. J. Damage Mech. 19 (1), 3–52.
Brocks, W., Sun, D.-Z., Hönig, A., 1995. Verification of the transferability of micromechanical parameters by cell model calculations with visco-plastic materials. Int. J. Plast. 11 (8), 971–989.
Chew, H., Guo, T., Cheng, L., 2007. Pressure-sensitive ductile layers – I. Modeling the growth of extensive damage. Int. J. Solids Struct. 44 (7–8), 2553–2570.
Chu, C., Needleman, A., 1980. Void nucleation effects in biaxially stretched sheets. J. Eng. Mater. Technol. 102 (3), 249–256.
Fabrègue, D., Pardoen, T., 2008. A constitutive model for elastoplastic solids containing primary and secondary voids. J. Mech. Phys. Solids 56 (3), 719–741.
Forest, S., 2009. Micromorphic approach for gradient elasticity, viscoplasticity, and damage. J. Eng. Mech. 135 (3), 117–131.
Gao, X., Kim, J., 2006. Modeling of ductile fracture: significance of void coalescence. Int. J. Solids Struct. 43 (20), 6277–6293.
Gao, X., Wang, T., Kim, J., 2005. On ductile fracture initiation toughness: effects of void volume fraction, void shape and void distribution. Int. J. Solids. Struct. 42 (18–19), 5097–5117.
Gross, D., Seelig, T., 2006. Fracture Mechanics – With an Introduction to Micromechanics. Springer.
Gu, I., 2000. Finite element analyses of deformation around holes near a crack tip and their implications to the J-resistance curve. Fatigue Fract. Eng. M. 23 (11), 943–952.
Gurson, A.L., 1977. Continuum Theory of ductile rupture by void nucleation and growth: part I – yield criteria and flow rules for porous ductile media. J. Eng. Mater. Technol. ASME 99 (1), 2–15.
Hütter, G., 2013. Multi-scale simulation of crack propagation in the ductile-brittle transition region (dissertation), TU Bergakademie Freiberg.
Hütter, G., Zybell, L., Mühlich, U., Kuna, M., 2012. Ductile crack propagation by plastic collapse of the intervoid ligaments. Int. J. Fract. 176, 81–96.
Hütter, G., Zybell, L., Mühlich, U., Kuna, M., 2013. Consistent simulation of ductile crack propagation with discrete 3D voids. Comput. Mater. Sci. 80, 61–70.
Hütter, G., Linse, T., Mühlich, U., Kuna, M., 2013. Simulation of ductile crack initiation and propagation by means of a non-local GTN-model under small-scale yielding. Int. J. Solids Struct. 50, 662–671.
Koplik, J., Needleman, A., 1988. Void growth and coalescence in porous plastic solids. Int. J. Solids Struct. 24 (8), 835–853.
Linse, T., Hütter, G., Kuna, M., 2012. Simulation of crack propagation using a gradient-enriched ductile damage model based on dilatational strain. Eng. Fract. Mech. 95, 13–28.
McMeeking, R.M., 1977. Finite deformation analysis of crack-tip opening in elastic-plastic materials and implications for fracture. J. Mech. Phys. Solids 25 (5), 357–381.
Needleman, A., Tvergaard, V., 1987. An analysis of ductile rupture modes at a crack tip. J. Mech. Phys. Solids 35 (2), 151–183.
Niordson, C.F., Tvergaard, V., 2007. Size-effects in porous metals. Model. Simul. Mater. Sci. 15 (1), S51–S60.
Perrin, G., Leblond, J., 1990. Analytical study of a hollow sphere made of plastic porous material and subjected to hydrostatic tension-application to some problems in ductile fracture of metals. Int. J. Plast. 6 (6), 677–699.
Petti, J.P., Dodds Jr., R.H., 2005. Ductile tearing and discrete void effects on cleavage fracture under small-scale yielding conditions. Int. J. Solids. Struct. 42 (13), 3655–3676.
Rice, J., Drugan, W., Sham, T., 1980. Elastic-plastic analysis of growing cracks. In: ASTM. STP, pp. 189–221.
Seidenfuss, M., Samal, M., Roos, E., 2011. On critical assessment of the use of local and nonlocal damage models for prediction of ductile crack growth and crack path in various loading and boundary conditions. Int. J. Solids Struct. 48 (24), 3365–3381.
Sreeramulu, K., Biswas, P., Narasimhan, R., Mishra, R., 2013. Ductile fracture by multiple void growth and interaction ahead of a notch tip in polycrystalline plastic solids. Int. J. Fract. 180 (2), 145–161.
Tian, R., Chan, S., Tang, S., Kopacz, A.M., Wang, J.-S., Jou, H.-J., Siad, L., Lindgren, L.-E., Olson, G.B., Liu, W.K., 2010. A multiresolution continuum simulation of the ductile fracture process. J. Mech. Phys. Solids 58 (10), 1681–1700.
Tvergaard, V., 1981. Influence of voids on shear band instabilities under plane strain conditions. Int. J. Fract. 17 (4), 389–407.
Tvergaard, V., 1982. Ductile fracture by cavity nucleation between larger voids. J. Mech. Phys. Solids 30 (4), 265–286.
Tvergaard, V., 1982. On localization in ductile materials containing spherical voids. Int. J. Fract. 18 (4), 237–252.
Tvergaard, V., 1989. Material failure by void growth to coalescence. Adv. Appl. Mech. 27, 83–151.
Tvergaard, V., 2007. Discrete modelling of ductile crack growth by void growth to coalescence. Int. J. Fract. 148 (1), 1–12.
Tvergaard, V., Hutchinson, J.W., 2002. Two mechanisms of ductile fracture: void by void growth versus multiple void interaction. Int. J. Solids. Struct. 39 (13–14), 3581–3597.
Tvergaard, V., Needleman, A., 1984. Analysis of the cup-cone fracture in a round tensile bar. Acta. Metall. Mater. 32 (1), 157–169.
Tvergaard, V., Needleman, A., 1995. Effects of nonlocal damage in porous plastic solids. Int. J. Solids Struct. 32 (8–9), 1063–1077.
Tvergaard, V., Needleman, A., 2006. Three dimensional microstructural effects on plane strain ductile crack growth. Int. J. Solids Struct. 43 (20), 6165–6179.
Tvergaard, V., Niordson, C.F., 2008. Size effects at a crack-tip interacting with a number of voids. Philos. Mag. 88 (30–32), 3827–3840.
Vernerey, F.J., Liu, W.K., Moran, B., Olson, G., 2008. A micromorphic model for the multiple scale failure of heterogeneous materials. J. Mech. Phys. Solids 56 (4), 1320–1347.
Zybell, L., Hütter, G., Linse, T., Mühlich, U., Kuna, M., in press. Size effects in ductile failure of porous materials containing two populations of voids. Eur. J. Mech. A-Solid., http://dx.doi.org/10.1016/j.euromechsol.2013.11.006.